Title
An Improved Polarflex Water Model

Journal
The Journal of Chemical Physics, 118

Authors
Jeon, Jonggu
Lefohn, Aaron
Voth, Greg

Publication Date
2003

Peer reviewed

An improved Polarflex water model

Jonggu Jeon, Aaron E. Lefohn, and Gregory A. Voth

Department of Chemistry and Henry Eyring Center for Theoretical Chemistry,

315 S. 1400 E. Rm 2020, University of Utah, Salt Lake City, Utah 84112-0850

Abstract

The three-site polarizable and flexible water potential employing the multistate empirical valence bond (MS-EVB) description for the electronic polarizability [A. E. Lefohn, M. Ovchinnikov and G. A. Voth, J. Phys. Chem. **105**, 6628 (2001)] has been modified for better reproduction of liquid water properties under ambient conditions. The improvement of the potential model was accomplished by (i) replacing the point charge distribution associated with the atomic interaction sites in the original model with a diffuse Gaussian charge distribution and (ii) reparameterizing the molecular geometry, components of electronic polarizability tensor, the Lennard-Jones parameters, and the widths of the Gaussian charge distribution. Static and dynamic properties, such as the intermolecular interaction energy, radial distribution function, diffusion constant, and dielectric constant, have been used in the model parameterization and the resulting model well reproduces the experimental data. A closely related rigid version of the model is also developed and compared with the flexible one. For computational efficiency, the extended Lagrangian algorithm for the electronic degrees of freedom has been implemented in the MS-EVB molecular dynamics simulation and utilized in the calculations. Relations between the new features of the potential model, such as the Gaussian charge distribution and the anisotropy in the electronic polarizability, and the liquid properties are estabilished and discussed.

I. INTRODUCTION

An accurate interaction potential model is essential to the molecular level understanding of physical and chemical phenomena in condensed-phase water. Simple potential models employing rigid geometry and fixed point charge distribution have been used in simulation studies[1] and have provided considerable insight into the molecular origin of the unique behavior of water in various phases and its role as a solvent.[2] These rigid, nonpolarizable potential models, however, do not capture the molecular charge redistribution in response to the environment[3] and the intramolecular atomic motions. While there exist a small number of water potential models that incorporate these polarizability and flexibility effects,[4–12] their applicability in liquid state simulation is often limited by insufficient liquid property characterization or their high computational demand.

Another important role of water in solution phase is as a proton donor or acceptor in acid-base reactions. Here, the transfer of a proton requires that the potential model for water be able to describe the O-H bond breaking and formation. The empirical valence bond (EVB) method[13] has beed applied to this problem and shown to be a simple and effective way to model the reaction system in aqueous solution.[14–17] In light of this and other successful applications of the EVB method to the study of chemical reactions,[18,19] the development of a polarizable water potential model employing the same EVB approach would lead to a unified description of the intra- and intermolecular electronic structure variation with high efficiency and accuracy. The "Polarflex" model,[20] a three-site flexible and polarizable water model employing the multistate EVB (MS-EVB) method for the description of the electronic polarizability, was developed for this purpose.

In this paper, we extend the original Polarflex model to provide a better description of water at ambient liquid state conditions. The basic MS-EVB description of the molecular electronic polarization will be retained. Even though the current model is focused on the correct reproduction of molecular ground-state electric properties, such as dipole moment and electronic polarizability, we note that the same approach has been applied to the liquid-state electronic spectroscopy[21,22] through a consistent description of solvent excited states.[23–25] Also, it can be extended in a straightforward way for a more refined electronic structure and hyperpolarizability description[26] and to the chemical reactions involving multiple electronic potential energy surfaces. When compared to more elaborate *ab initio* molecular dynam-

ics methods now available,[27,28] the MS-EVB approach has certain advantages in terms of computational efficiency and transparent interpretation of results.

The improvement of the original Polarflex water model is achieved in two ways. First, we employ the diffuse Gaussian charge distribution (GCD) for the interaction sites instead of the more conventional point charge description. The point charge distribution has been used in the majority of existing water potential models due to its simplicity. However, the short range interactions from such models tend to be overestimated due to the divergent character of point charge interactions at small separation. This becomes more severe with polarizable models that employ variable charge sites. For this reason, the Gaussian or other types of diffuse charge distributions have been employed previously for inter- or intramolecular interactions.[9,29–31] We employ the GCD for the evaluation of the intermolecular electrostatic interactions involving the three atomic sites. Second, the model parameters, including the equilibrium geometry, individual components of the polarizability tensor, the Lennard-Jones (LJ) potential parameters, are optimized together with the widths of the GCD with the goal of reproducing a set of experimental properties of ambient liquid water. In the parameterization, the oxygen-oxygen radial distribution function and the self-diffusion constant were chosen as the initial target properties. In addition, the intermolecular interaction energy and the static dielectric constant were monitored so that the model provides a good description of these properties as well. In order to isolate and study the effect of flexibility, we have also developed a new rigid version of the MS-EVB water model which resembles the flexible one in many aspects. Hereafter, the rigid model will be called Polarflex Rigid Gaussian (PRG) and the flexible one, Polarflex Flexible Gaussian (PFG).

The modeling of intramolecular flexibility within the MS-EVB framework requires careful consideration. Since the molecular charge distribution is represented by partial charges associated with atomic sites, the atomic motion will affect the former, and the electronic polarizability is coupled to the intramolecular motion.[6,32] In this study, we ignore any explicit coupling of this kind and formulate the MS-EVB electronic polarizability at the equilibrium geometry of the molecule. As a result, the MS-EVB Hamiltonian for an isolated molecule is independent of the geometry of the molecule in our description. While this approximation is expected to be reasonable considering the small amplitude of vibrational ground state motions in a pure water system,[33] we note that the flexibility of the molecule could be integrated in the MS-EVB polarizability for an even better description of charge distribution

of a flexible water molecule[10,34] in the future.

The current MS-EVB water model, and most other polarizable models, require a computationally expensive iteration in order to ensure self-consistency in the system charge distribution. In order to avoid this iteration and improve the computational efficiency, we have developed an extended Lagrangian algorithm for the EVB degrees of freedom in a molecular dynamics (MD) simulation. This algorithm provides a good approximation to the self-consistent solution associated with the polarizability and is compulationally efficient (i.e., only 10 % more expensive than a nonpolarizable model [Section IV]).

This paper is organized as follows. In Section II, we present the theoretical background of the MS-EVB water model, including results relevant for GCD. In Section III, the rigid (PRG) and flexible (PFG) MS-EVB potential models are described in detail and Sec. IV provides the computational details. The calculated properties of the two potential models are then presented in Section V. Finally, we discuss various related issues in Section VI.

II. THEORY

We first briefly review the MS-EVB method applied to the description of the electronic polarizability of a water molecule.[20,23,35] The Hamiltonian and the Schrödinger equation for the system of condensed-phase water are then developed employing the MS-EVB water model. Explicit expressions for Gaussian interaction-site charge distribution are presented next, and we then describe the extended Lagrangian algorithm for the treatment of the system electronic polarizability within the MS-EVB framework.

A. MS-EVB description of the electronic polarizability

We consider an isolated water molecule represented by three atomic interaction sites. The electronic structure of the molecule is spanned by three orthonormal basis states constructed from possible charge fluctuations in the liquid phase. They are shown in Fig. 1 and will be called the EVB basis set, $B_{\rm EVB}$, collectively,

$$\begin{aligned} B_{\rm EVB} &= \{|1\rangle, |2\rangle, |3\rangle\} \; ; \\ \langle m|n\rangle &= \delta_{mn} \; (m, n = 1, 2, 3), \end{aligned} \tag{2.1}$$

where δ_{mn} is the Kronecker delta function. In this basis, the molecular geometry is assumed to be fixed at its equilibrium values. The partial charge distribution on an atomic site α is represented by a charge density operator $\hat{\rho}_\alpha(\mathbf{r})$ centered at the atomic position $\mathbf{r}_\alpha$ ($\alpha = \mathrm{O},\ \mathrm{H}_1,\ \mathrm{H}_2$) and its expectation value $\rho_\alpha^n(\mathbf{r})$ for EVB basis state $|n\rangle$,

$$\langle m|\hat{\rho}_\alpha(\mathbf{r})|n\rangle = \delta_{mn}\rho_\alpha^n(\mathbf{r}). \tag{2.2}$$

We also introduce the charge operator $\hat{q}_\alpha$ and its expectation value q_α^n defined by

$$\hat{q}_\alpha = \int d\mathbf{r}\ \hat{\rho}_\alpha(\mathbf{r})\ ; \qquad \langle m|\hat{q}_\alpha|n\rangle = \delta_{mn}q_\alpha^n\ . \tag{2.3}$$

We obtain three $C_{2\mathrm{v}}$-symmetry adapted eigenstates,[20] ψ_i's, for the water molecule from B_{EVB},

$$\begin{aligned}
\psi_1 &= -C|1\rangle + \frac{S}{\sqrt{2}}\left(|2\rangle + |3\rangle\right)\ :\ A_1 \\
\psi_2 &= S|1\rangle + \frac{C}{\sqrt{2}}\left(|2\rangle + |3\rangle\right)\ :\ A_1 \\
\psi_3 &= \frac{1}{\sqrt{2}}\left(|2\rangle - |3\rangle\right)\ :\ B_1,
\end{aligned} \tag{2.4}$$

where $S^2 + C^2 = 1$ and A_1 and B_1 are irreducible representations of the $C_{2\mathrm{v}}$ group to which the eigenstates belong. The electronic Hamiltonian of the molecule $\hat{h}^0$ is diagonal when expressed in these eigenstates,

$$h_{ij}^0 \equiv \langle\psi_i|\hat{h}^0|\psi_j\rangle = \delta_{ij}E_i\ , \tag{2.5}$$

where E_i is the energy eigenvalue associated with the eigenstate ψ_i.

We complete the specification of the electronic structure of the molecule by determining the unknown parameters in Eqs. (2.4) and (2.5) from empirical data of dipole moment $\boldsymbol{\mu}^0$ and electronic polarizability $\boldsymbol{\alpha}^0$ for an isolated water molecule. The expressions for $\boldsymbol{\mu}^0$ and $\boldsymbol{\alpha}^0$ of the molecule in its ground electronic state (ψ_1) are given by

$$\begin{aligned}
\boldsymbol{\mu}^0 &= \langle\psi_1|\hat{\boldsymbol{\mu}}|\psi_1\rangle = \sum_\alpha \mathbf{r}_\alpha\langle\psi_1|\hat{q}_\alpha|\psi_1\rangle\ , \\
\boldsymbol{\alpha}^0 &= 2\sum_{i=2}^{3}\frac{\langle\psi_i|\hat{\boldsymbol{\mu}}|\psi_1\rangle\langle\psi_1|\hat{\boldsymbol{\mu}}|\psi_i\rangle}{E_i - E_1} \\
&= 2\sum_\alpha\sum_\beta \mathbf{r}_\alpha\mathbf{r}_\beta\sum_{i=2}^{3}\frac{\langle\psi_i|\hat{q}_\alpha|\psi_1\rangle\langle\psi_1|\hat{q}_\beta|\psi_i\rangle}{E_i - E_1}\ ,
\end{aligned} \tag{2.6}$$

where α and β are atomic site indices and $\hat{\boldsymbol{\mu}} = \sum_\alpha \hat{q}_\alpha \mathbf{r}_\alpha$. By supplying empirical data on the left-hand side of Eq. (2.6), the unknown parameters S, $E_2 - E_1$, and $E_3 - E_1$ are uniquely determined. Since the out-of-plane component of $\boldsymbol{\alpha}$ cannot be described by the current 3-site water model, only the two in-plane components are used in this procedure. The quantities S, E_2, and E_3 (with $E_1 \equiv 0$) specify the gas-phase eigenstates [Eq. (2.4)] and the electronic Hamiltonian [Eq. (2.5)]. We can express $\hat{h}^0$ in the EVB basis set as a nondiagonal 3×3 matrix $h^0_{\rm EVB}$ after the transformation defined by Eq. (2.4). The electronic structure and the electric properties of an isolated water molecule are completely determined by $B_{\rm EVB}$ and $h^0_{\rm EVB}$ in the 3-site MS-EVB description. Since this parameterization is based on the equilibrium geometry of an isolated water molecule, the flexibility of the molecule, to be introduced below via a separate classical potential, does not affect $h^0_{\rm EVB}$.

B. System Hamiltonian and self-consistent field approximation

The Hamiltonian for a system of N water molecules are given as

$$\hat{H} = \hat{H}^0 + \hat{H}_{\rm Coul} + K + V_{\rm LJ} + V_{\rm Intra} \ , \tag{2.7}$$

where $\hat{H}^0$ is the sum of molecular electronic Hamiltonians introduced in Eq. (2.5), $\hat{H}_{\rm Coul}$ is the intermolecular Coulombic interaction, K is the kinetic energy, $V_{\rm LJ}$ is the Lennard-Jones interaction, and $V_{\rm Intra}$ is the classical intramolecular potential. Even though the MS-EVB model is, in principle, capable of describing the intermolecular dispersion interaction, the self-consistent field approximation employed in the following development lacks the intermolecular correlation effect necessary for such a description.[23] Therefore, we describe the dispersion interaction by the conventional Lennard-Jones potential, leaving the full quantum description of this type of interaction for future study. The last three terms on the right-hand side of Eq. (2.7) depend only on the atomic positions and velocities and therefore are treated classically as c-numbers. On the other hand, $\hat{H}^0$ and $\hat{H}_{\rm Coul}$ are quantum mechanical operators given by

$$\begin{aligned} \hat{H}^0 &= \sum_{i=1}^{N} \hat{h}^0_i \ , \\ \hat{H}_{\rm Coul} &= \frac{1}{2} \sum_{i=1}^{N} \sum_{\alpha} \sum_{\substack{j=1 \\ (j \neq i)}}^{N} \sum_{\beta} \int d\mathbf{r} \int d\mathbf{r}' \, \frac{\hat{\rho}_{i\alpha}(\mathbf{r}) \hat{\rho}_{j\beta}(\mathbf{r}')}{|\mathbf{r} - \mathbf{r}'|} \ , \end{aligned} \tag{2.8}$$

where i and j are molecular indices, $\hat{h}_i^0$ is the electronic Hamiltonian of molecule i introduced in Eq. (2.5), and the subscript $i\alpha$ stands for the site α of molecule i. We now construct the system wavefunction Ψ as a direct product of the molecular wavefunctions ψ^i analogous to the Hartree product in quantum chemistry, i.e.,

$$\Psi = \prod_{i=1}^{N} \psi^i \ ; \qquad E = \langle \Psi | \hat{H} | \Psi \rangle \ , \tag{2.9}$$

where E is the total energy of the system. Following the development of the Hartree-Fock equation in quantum chemistry,[23,36] we invoke the variational principle to E, that is, minimize E with respect to ψ^i under the normalization condition for ψ^i, to obtain a set of N coupled effective molecular Schrödinger equations,

$$\begin{aligned} \hat{h}^i_{\rm eff} |\psi^i\rangle &= \varepsilon^i |\psi^i\rangle \ ; \\ \hat{h}^i_{\rm eff} &= \hat{h}^0_i + \sum_{\alpha} \sum_{\substack{j=1 \\ (j\neq i)}}^{N} \sum_{\beta} \int d\mathbf{r} \int d\mathbf{r}' \, \frac{\langle \psi^j | \hat{\rho}_{j\beta}(\mathbf{r}) | \psi^j \rangle \hat{\rho}_{i\alpha}(\mathbf{r}')}{|\mathbf{r} - \mathbf{r}'|} \ . \end{aligned} \tag{2.10}$$

Once these equations are solved for the ground-state ε^i's and $|\psi^i\rangle$'s, the total energy of the system is obtained from the following relation

$$\begin{aligned} E = & \sum_{i=1}^{N} \varepsilon^i - \frac{1}{2} \sum_{i=1}^{N} \sum_{\alpha} \sum_{\substack{j=1 \\ (j\neq i)}}^{N} \sum_{\beta} \int d\mathbf{r} \int d\mathbf{r}' \, \frac{\langle \psi^i | \hat{\rho}_{i\alpha}(\mathbf{r}) | \psi^i \rangle \langle \psi^j | \hat{\rho}_{j\beta}(\mathbf{r}') | \psi^j \rangle}{|\mathbf{r} - \mathbf{r}'|} \\ & + K + V_{\rm LJ} + V_{\rm Intra} \ . \end{aligned} \tag{2.11}$$

In practice, the molecular Schrödinger equations in Eq. (2.10) can be solved iteratively to achieve self-consistency in the charge distribution among N molecules or be treated approximately with the extended-Lagrangian algorithm [Section II D].

When periodic boundary conditions and the Ewald summation method are employed, it is necessary to take into account the contributions from periodic images. We consider this in the next section after we specify the atomic charge distribution $\rho^n_\alpha(\mathbf{r})$ introduced in Eq. (2.2).

C. Gaussian charge distributions

In many force fields employed in MD simulations, it is usual to represent the partial charges on interaction sites by point charges. While the point charge model is a simple

and efficient way to represent the leading-order multipole moments of the molecular charge distribution, the short-range interactions in such a model may be too strong considering the diffuse character of the actual electronic charge distribution. This was evident in our initial MS-EVB water model (Polarflex),[20] which employed the point charge model. In that study, the introduction of polarizability through the MS-EVB description resulted in improvements in the interaction energy and the hydrogen bond structure, as indicated by the second peak of the oxygen-oxygen radial distribution function (RDF) when compared to the results of its nonpolarizable counterpart, the SPC/F model.[37] However, the first peak of the oxygen-oxygen RDF was enhanced too much and the calculated diffusion constant was smaller than the experimental data, indicating that the short-range electrostatic interaction may be somewhat overestimated. In order to overcome these disadvantages, we employ here the diffuse Gaussian charge distribution instead of the point charges used in our previous study.

In the Gaussian charge distribution (GCD) model, the charge density operator $\hat{\rho}_\alpha(\mathbf{r})$ associated with the atom α [Eq. (2.2)] becomes

$$\hat{\rho}_\alpha(\mathbf{r}) = (2\pi\xi_\alpha^2)^{-3/2}\hat{q}_\alpha \exp\left[-\frac{|\mathbf{r}-\mathbf{r}_\alpha|^2}{2\xi_\alpha^2}\right] , \tag{2.12}$$

where ξ_α is the width (standard deviation) of the Gaussian distribution. We assume that ξ_α are identical for the same kind of atoms. Two GCD's $\rho_\alpha^n(\mathbf{r})$ and $\rho_\beta^m(\mathbf{r})$, obtained from Eqs. (2.2) and (2.12), interact with each other with the interaction energy $E_{\alpha\beta}^{nm}$ given by

$$E_{\alpha\beta}^{nm} = \frac{q_\alpha^n q_\beta^m}{|\mathbf{r}_\alpha - \mathbf{r}_\beta|}\,\mathrm{erf}\left[\frac{|\mathbf{r}_\alpha - \mathbf{r}_\beta|}{\sqrt{2(\xi_\alpha^2+\xi_\beta^2)}}\right] , \tag{2.13}$$

where q_α^n is defined by Eq. (2.3) and erf is the error function. The treatment of the long-range electrostatic interactions in this method are described in Appendix A.

D. Extended Lagrangian method for MS-EVB Molecular Dynamics

The computational demand of the MD simulation of Polarflex water using the self-consistent iteration algorithm is about 2.5 times higher than that of its nonpolarizable counterpart, the SPC/F model.[37] The additional computation is required for the iterative solution of the molecular Schrödinger equations until the self-consistency in the charge distribution is achieved. In order to improve the computational efficiency, we have adapted the

extended Lagrangian (ext-L) algorithm[27,28,38,39] for the MS-EVB degrees of freedom in the MD simulation. In the ext-L method, a small mass is assigned to the system electronic degrees of freedom and its kinetic energy is included in the system Lagrangian. The equations of motion for the electronic degrees of freedom resulting from the Lagrangian are then solved along with the equations for the nuclear motion. The electronic degrees of freedom thereby follow closely the actual solution so long as they are adiabatically separated from the nuclear motions. This scheme enables us to avoid the expensive iteration steps and achieve a high computational efficiency. In what follows, we develop the ext-L formulation appropriate for the MS-EVB method. Our development is based on the GCD model and the Ewald sum for the Coulombic interaction. The basic algorithm is adapted from the RATTLE-like algorithm proposed by Tuckerman and Parrinello[40] based on the velocity Verlet integration method.[41]

We first expand the ground-state molecular wavefunctions ψ^i in the EVB basis states $|n\rangle$,

$$\psi^i = \sum_n c_n^i |n\rangle \ , \tag{2.14}$$

and we take c_n^i's as real numbers. The system total energy in Eq. (2.11), expressed in terms of the EVB basis states, can then be regarded as a function of the positions of the atomic sites, their time derivatives, and the expansion coefficients of the wavefunctions

$$E = E(\{\mathbf{r}_{i\alpha}\}, \{\dot{\mathbf{r}}_{i\alpha}\}, \{c_n^i\}) = K(\{\dot{\mathbf{r}}_{i\alpha}\}) + V(\{\mathbf{r}_{i\alpha}\}, \{c_n^i\}) \ , \tag{2.15}$$

where $\dot{\mathbf{r}}$ denotes time derivative of $\mathbf{r}$ and $V = \langle\Psi|\hat{H}^0|\Psi\rangle + E_{\rm Coul} + V_{\rm LJ} + V_{\rm Intra}$ [*cf.* Eq. (A6)]. We assign a small mass m_c to the c_n^i's and consider the resulting kinetic energy $K_{\rm ext}$

$$K_{\rm ext}(\{\dot{c}_n^i\}) = \frac{1}{2} m_c \sum_{i=1}^{N} \sum_n |\dot{c}_n^i|^2 \ . \tag{2.16}$$

The dynamics of the system including that of c_n^i's is governed by the extended Lagrangian $L_{\rm ext}$

$$L_{\rm ext} = K(\{\dot{\mathbf{r}}_{i\alpha}\}) + K_{\rm ext}(\{\dot{c}_n^i\}) - V(\{\mathbf{r}_{i\alpha}\}, \{c_n^i\}) + \sum_{i=1}^{N} \Lambda_i (\sum_n |c_n^i|^2 - 1) \ , \tag{2.17}$$

where the last term involves the Lagrangian multipliers Λ_i to ensure the normalization of the ground state wavefunction ψ^i. The equations of motion for c_n^i's are obtained from $L_{\rm ext}$

as

$$
\begin{aligned}
m_c \ddot{c}_n^i &= \frac{\partial L_{\rm ext}}{\partial c_n^i} \\
&= -2\sum_m c_m^i (h^0_{\rm EVB})_{mn} - 2c_n^i \sum_\alpha q_\alpha^n \Phi_{i\alpha}(\mathbf{r}_{i\alpha}) + 2\Lambda_i c_n^i \\
&= -2\sum_m c_m^i (\hat{h}^i_{\rm eff})_{mn} + 2\Lambda_i c_n^i \ , \qquad (2.18)
\end{aligned}
$$

where $(h^0_{\rm EVB})_{mn} = \langle m|\hat{h}^0|n\rangle$ and is identical for all molecules in the system, $(\hat{h}^i_{\rm eff})_{mn} = \langle m|\hat{h}^i_{\rm eff}|n\rangle$, and the last identity comes from Eqs. (A4) and (A5). The numerical algorithm for integrating these equations is described in Appendix B.

III. POTENTIAL MODELS

In this section, we describe the Polarflex flexible three-site water potential model (PFG) employing the MS-EVB description of electronic polarizability and the Gaussian charge distribution. For comparison, we also construct a closely related rigid version of the model (PRG). The properties of liquid water using these models are then presented in the following sections.

For both PRG and PFG models, the short-range dispersion-repulsion interactions are described by the LJ potential between oxygen atoms only

$$
V_{\rm LJ} = \frac{1}{2}\sum_{i=1}^{N}\sum_{\substack{j=1 \\ (j\neq i)}}^{N} 4\epsilon \left[\left(\frac{\sigma}{r_{i{\rm O},j{\rm O}}}\right)^{12} - \left(\frac{\sigma}{r_{i{\rm O},j{\rm O}}}\right)^{6} \right] \ , \qquad (3.1)
$$

where the parameters ϵ and σ are given for each model in Table I.

For the PFG model, we have attempted to optimize the geometry, the widths of the Gaussian charge distribution, and the LJ interaction parameters with the goal of reproducing the experimental oxygen-oxygen radial distribution function and self-diffusion constant under an ambient condition. The intermolecular interaction energy and dielectric constant were also monitored in order to identify and discard models with large deviations of these properties from experimental data. In addition, recognizing the anisotropic change in polarizability as the molecule deforms in the liquid (see Appendix C), we have individually adjusted the two in-plane polarizability components, α_{yy} and α_{zz} (with the molecule on the yz-plane and the molecular axis in the z direction). The parameters for the rigid PRG model were mainly

determined with the same principle. However, some of its parameters were taken from the PFG model in order to facilitate direct comparison between the two models.

A. Rigid model (PRG)

First, we specify the geometry, dipole moment, and in-plane polarizability necessary for the characterization of the electronic ground state of an MS-EVB water molecule. These input values are given in Table I and used to obtain the single-molecule electronic Hamiltonian $h^0_{\rm EVB}$ according to the prescription of Section II A. We employed the OH bond length of 1.0 Å, the value of the SPC model.[42] The bond angle $\angle$HOH was taken as 107.47°, a decrease from the SPC value of 109.47°, so that it is close to the average liquid-phase geometry of the flexible PFG model described below. Likewise, a slightly increased OH bond length of 1.02 Å was tried but rejected since it lead to higher dielectric constant in liquid. The dipole moment and electronic polarizability of an isolated molecule were taken from experimental values.[43,44] The out-of-plane component of the polarizability cannot be modeled by the three site model and was ignored. Also given in Table I are the widths of the GCD ξ_α and parameters for the LJ interaction between oxygen atoms. The widths of the GCD are the optimal values for the flexible model described below. Finally, the LJ parameters for the SPC model were employed without modification since these values, in combination with other parameters, produced a reasonable interaction energy in liquid.

B. Flexible model (PFG)

In principle, flexibility can be incorporated in the MS-EVB formulation by modeling the internal vibration of the EVB basis states empirically so that the resulting ground state potential energy surface reproduces a target surface. In this study, however, we take a simpler approach originating in Ref. 20. Here, we assume that the molecular electronic Hamiltonian $\hat{h}^0$ [Eq. (2.5)] is independent of atomic positions and its representation in the EVB basis set, $h^0_{\rm EVB}$, remains constant regardless of molecular deformation once it is determined from the equilibrium geometry as described in Section II A. The potential energy surface of a molecule is separately modeled by a classical potential function. For this purpose, we

employ the harmonic potential function of Toukan and Rahman[37] given by

$$V_{\text{Intra}} = \frac{1}{2}a\left[(\Delta r_{\text{OH}_1})^2 + (\Delta r_{\text{OH}_2})^2\right] + \frac{1}{2}b(\Delta r_{\text{H}_1\text{H}_2})^2 + c(\Delta r_{\text{OH}_1} + \Delta r_{\text{OH}_2})\Delta r_{\text{H}_1\text{H}_2} + d\Delta r_{\text{OH}_1}\Delta r_{\text{OH}_2} \ , \tag{3.2}$$

where $\Delta r_{\alpha\beta} = r_{\alpha\beta} - r^0_{\alpha\beta}$ with $r^0_{\alpha\beta}$ the equilibrium distance between atoms α and β in the gas phase and the force constants a, b, c, and d are given in Table II. Also shown there are the vibrational frequencies of an isolated molecule at 1 K, determined from the Fourier transform of atomic velocity trajectories.[45] The frequencies at 300 K agree with the 1 K values within 1 cm^{-1}. We note that the vibrational frequencies of the model function do not agree exactly with the experimental values since the parameters of the Toukan-Rahman potential were determined from the "harmonic" frequencies.[46,47] There is also a small change in frequencies from the Toukan-Rahman model, especially for the bending mode, due to the different equilibrium geometry employed. As we can see from the molecular Schrödinger equation [Eqs. (2.10) and (A4)], the intramolecular motion is coupled to the electronic degrees of freedom in the condensed phase through the intermolecular Coulombic interaction.

Other parameters of the PFG model are shown in Table I. The equilibrium geometry of an isolated water molecule is taken as $r^0_{\text{OH}} = 1.0$ Å and $(\angle\text{HOH})^0 = 112°$. The OH bond length is identical to that for SPC model and the HOH angle is increased from the SPC value in order to improve the calculated dielectric constant in the liquid [Section V B 4]. As in the PRG model, the dipole moment μ^0 of an isolated molecule is taken to be the experimental value of 1.855 D. The polarizability components employed for an isolated molecule are $\alpha^0_{yy} = 1.2928$ Å^3 and $\alpha^0_{zz} = 0.9542$ Å^3, corresponding to 84.6 and 65.0 % of the gas-phase experimental values, respectively. As explained in Appendix C, α_{zz} is enhanced in the liquid to a larger extent than α_{yy} as a result of the change in average molecular geometry. Therefore, the anisotropic scaling of polarizability components as applied here for the isolated molecule would result in near isotropic polarizability in liquid at approximately 80 % of the gas-phase experimental value. A further discussion on the effects of polarizability anisotropy on properties will be given in Section VI.

The widths of the Gaussian charge distribution are specified to be 0.8 Å both for the oxygen and hydrogen sites. Due to the large number of parameters subjected to optimization and their interrelation with regard to the computed properties, it is very difficult to determine a unique value of the Gaussian width. However, the current choice is in line with

previous water modeling studies that have employed Gaussian charge distribution[29,48,49] and produces a reasonable set of properties when used in combination with other model parameters. We have also tried differing Gaussian widths for the oxygen and hydrogen sites. In principle, this provides even better control over the short-range interactions between different kinds of atomic sites. However, in the current model, it did not result in a significant improvement and was therefore discarded for the sake of simplicity.

The LJ parameters for PFG has a larger σ (3.215 Å) and a smaller ϵ (0.139896 kcal/mol) value than the SPC values ($\sigma = 3.165$ Å and $\epsilon = 0.15544$ kcal/mol). Therefore, the model exhibits a stronger repulsion and slightly weaker dispersion interaction compared to the SPC water. This choice was mainly governed by the enhanced interactions arising from the induced dipole moments. With this choice, the oxygen-oxygen radial distribution function, sensitive to the LJ parameters, is found to have good positions of the first and second peaks [Section V B 2].

The quadrupole moment of an isolated molecule derived from the geometry and dipole moment is shown also in Table I for the two models. These values are sensitive to the value of the HOH bond angle and are underestimated compared to the experimental data. This is a general limitation of a 3-site modeling of water and cannot be significantly improved unless additional interaction charge sites are introduced in the model.

IV. MD SIMULATION DETAILS

Liquid phase MD simulations were carried out with 256 water molecules in a cubic box of length $L = 19.73$ Å, corresponding to a density of 0.997 g/cm^3. The velocity Verlet algorithm[41] was employed to integrate the atomic equations of motion with time step size of 0.5 fs (PFG) or 1.0 fs (PRG). The system was initially equilibrated at ~ 300 K for more than 100 ps. The simple velocity scaling method was used to control the system temperature during this equilibration stage. The production runs were then carried out in the micro-canonical ensemble without velocity scaling or thermostat. Periodic boundary conditions were imposed. For short-range LJ interactions, all minimum image pairs were included in the potential and force calculations. For the calculation of electrostatic interactions, the Ewald sum method was employed with the conducting boundary condition [Appendix A]. The width of the Gaussian screening charge distribution ξ_s was chosen as 2.18 Å and the

k-space summations were truncated such that $n^2 \leq 54$ and $n_\alpha \leq 8$, where $\mathbf{n} = L\mathbf{k}/(2\pi)$. The value of ξ_s corresponds to $\kappa_{\alpha s} = 6.4/L$ in the point charge limit ($\xi_\alpha = 0$) [Eq. (A2)].

In this study, we have used both the iteration method[20] and the extended Lagrangian method [Section II D] to treat the MS-EVB electronic degrees of freedom. For the iteration method, we used a relative convergence criterion of 10^{-12} in terms of the total energy. With this, convergence was achieved in 7–8 (PFG) and 9–10 (PRG) iterations and the total energy was conserved within 0.001 kcal/mol/100 ps. In the extended Lagrangian calculation, we determined the smallest possible values of the fictitious mass m_c which did not cause numerical instabilities. The optimal values are found to be 108 au ([energy]×[time]^2) for PFG and 390 au for PRG. With these values, the total energy of the real system [Eq. (2.15)] is conserved within 0.0005 kcal/mol/100 ps. We note that the energy conservation with the rigid model is 2–4 times better than that with the flexible model for a given integration method. This is likely due to more degrees of freedom and faster intramolecular motions present in the PFG model. Even though the ext-L method results in a better energy conservation than the iteration for a short trajectory ($\leq$ 400 ps for PRG, $\leq$ 200 ps for PFG), the kinetic energy $K_{\rm ext}$ of the fictitious electronic degrees of freedom in the former will eventually become significant and the real system dynamics will be affected at longer times. Therefore, when a long trajectory is required, the ext-L simulation was truncated after 200 ps (PFG) or 400 ps (PRG) and resumed with a single iteration step in the beginning, resetting $K_{\rm ext}$ to zero. In addition, for both iteration and ext-L simulation, a short velocity scaling period ($\sim$ 2 ps) was inserted between production trajectories every 0.5–1 ns in order to maintain the target temperature of 300 K. The errors associated with the ext-L calculation will be discussed in Section VI.

The use of GCD instead of point charges incurs about 40 % increase in computational time for nonpolarizable models such as SPC and SPC/F. When the polarizability is also added to these, there is an additional factor of 1.1 (ext-L algorithm) or 2.5 (iteration algorithm) increase in computational time. As a result, the computational demand of the PRG model is 1.5 (with ext-L algorithm) and 3.5 (with iteration) times higher than that of the SPC model. Likewise, the PFG model is 1.6 (with ext-L algorithm) and 3.3 (with iteration) times more expensive than the SPC/F model. These modest increases in computational demand, especially for the ext-L approach, are quite encouraging for treating realistic systems.

V. RESULTS

A. Dimer properties

Even though the current MS-EVB water models were developed with the purpose of reproducing ambient liquid water properties, it is of interest to study their dimer properties because they indicate the phase-transferability of the model. The equilibrium geometry of the dimer cluster was obtained by gradual velocity scaling to the target temperature of 0.1 K. At this temperature, the kinetic energy of the system is negligible compared to the potential energy. In Table III, we have listed the equilibrium geometry and the dissociation energy obtained from the PRG and PFG models. From the O-O distance r_{OO} and the dissociation energy D_e, we note that PRG yields a slightly stronger intermolecular interaction than PFG. Aside from the small effect on the PFG dimer of the increased OH bond length (1.014Å) participating in the hydrogen bond, this effect is mainly due to the higher vacuum polarizability of the rigid model. This picture may also change in the liquid phase: since the average $\angle$HOH of PFG in liquid (107.39°, Section V B) is significantly smaller than that in dimer (110.6° for the hydrogen-bond donor and 110.9° for the acceptor), the effective molecular polarizabily of the flexible model will be higher in liquid than in dimer (see Appendix C) with the resulting increase in electrostatic interaction in liquid. The two MS-EVB water dimer results and the experimental data shows a good agreement in general. The only exception is the angle between the O-O axis and the symmetry axis of the acceptor molecule, θ_a, for which the two MS-EVB model predictions are much smaller than the experiment. This seems to be a general limitation of a three-site water model.[50–52] Nonetheless, the current models provide a distinctive improvement in dimer properties compared to nonpolarizable three-site potential models, such as SPC, SPC/E, and TIP3P.[50,51]

B. Properties in the liquid

1. Molecular properties

The average molecular geometry of the PFG model undergoes a significant change in going from gas phase to liquid. As shown in Table IV, the average OH bond length $\bar{r}_{\mathrm{OH}}$ increases by 0.02 Å and the average HOH bond angle $\overline{\angle \mathrm{HOH}}$ decreases by 4.6° from the equilibrium

values. While the increase of $\bar{r}_{\mathrm{OH}}$ is in agreement with experiment,[53] the large decrease of $\overline{\angle\mathrm{HOH}}$ contradicts experimental data[53] and theoretical results employing quantum chemical methods.[54–56] This problem is common in the majority of flexible water potential models and arises because the molecular charge distribution cannot adjust properly to the changing geometry. We address the consequences of this problem and possible solutions in Section VI. Despite this, $\overline{\angle\mathrm{HOH}}$ is within the range of experimental estimates thanks to the adjusted value of $(\angle\mathrm{HOH})^0$.

The average molecular dipole moments in liquid, $\bar{\mu}$, of the PRG and PFG models are 2.590 and 2.604 D, respectively. They are in line with many other polarizable water potential models.[24,30,57–60] We note that $\bar{\mu}$ of the PFG model is slightly higher than that of the PRG model even though the PRG model has a higher gas phase polarizability. As mentioned in the previous section and Appendix C, this is because the decrease of $\angle$HOH results in an enhanced polarizability (both electronic and atomic) for the PFG model in liquid.

2. Structure

The radial distribution functions of the PRG and PFG models are shown in Figs. 2–4 together with the results for the original Polarflex model[20] and data extracted from x-ray scattering[61] or neutron diffraction[62] experiments.

The oxygen-oxygen distribution g_{OO} [Fig. 2] was used in the parameterization of the PRG and PFG models. As a result, these models show very good agreement with the experimental g_{OO} of Sorenson et al.[61] in terms of the positions of the first peak and the position and height of the second peak. The height of the first peak is somewhat too high and the first minimum is located too low and inward for these models. These discrepancies could not be removed without an impact on the reproduction of other properties. We note that the overstructuring of the g_{OO} first peak is a general tendency of polarizable potential models[61] and was greatly improved by the employment of GCD in the current models instead of the point charges (the original Polarflex model shows a similar first peak height but its dipole moment in the liquid is about 0.05 D less than those of PFG and PRG.[20]). The coordination numbers of the first solvation shell obtained by integrating g_{OO} up to the first minimum are 4.0, 4.2, and 4.3 for the original Polarflex, PRG, and PFG model, respectively. These values compare favorably to the x-ray scattering result of 4.7 (Ref. 61) or the neutron diffraction result of 4.5 (Ref.

62). The lower values for the PRG and PFG models are another manifestation of stronger short-range interaction for these models. These values are very sensitive to the position of the first minimum and can be brought closer to the experimental data if the experimental minimum position (∼3.4 Å) instead of the model prediction (∼3.3 Å) is used as the upper limit of integration.

The oxygen-hydrogen and hydrogen-hydrogen radial distributions of the PRG and PFG models [Figs. 3 and 4] also show positions of the first and second peaks in good accord with the neutron diffraction results of Soper.[62] The peak heights are, on the other hand, overestimated compared to the experimental results. While this indicates that the short-range interactions are too strong, a comparison of classical g_{OH} and g_{HH} with experiment involves more uncertainty due to a significant nuclear quantum effect expected for the hydrogen atoms.[63,64]

3. Energetics

The intramolecular potential energy, V_{Intra}, of the PFG model in liquid is 1.79 kcal/mol and is 0.28 kcal/mol higher than the value for SPC/F (Table IV). This occurs because the stronger intermolecular interaction of polarized molecules favors more distortion of the PFG water geometry. This is a large increase from the gas-phase value at 300 K (0.93 kcal/mol for both SPC/F and PFG models, which is close to the harmonic value of 0.89 kcal/mol). We note that Stern and Berne[64] estimated quantum corrections to the intramolecular energy based on a harmonic oscillator model and found a value of −0.6 kcal/mol for the difference between the quantum corrections in the liquid and gas phase. If this is applied to the current result, the liquid state V_{Intra} of the PFG model would be much closer to the gas-phase value.

The intermolecular potential energy V_{Inter} of the PRG and PFG models are −10.02 and −10.56 kcal/mol, respectively (Table IV). This is higher than the SPC/F value of −11.36 kcal/mol. However, V_{Inter} for polarizable models include self-polarization energy given by $\sum_i[\langle\psi^i|\hat{h}_i^0|\psi^i\rangle - \langle\psi^i_{\mathrm{gas}}|\hat{h}_i^0|\psi^i_{\mathrm{gas}}\rangle]$ and the electrostatic part of V_{Inter} would in fact be much stronger for the polarizable models. The difference in the total potential energy V (= V_{Intra} + V_{Inter}) between the liquid and gas phase can be compared to the experimental configuration energy of −9.92 kcal/mol[50] and was actually monitored during the parameterization process. The PRG and PFG models show good agreement with the experimental value to within

~ 0.2 kcal/mol. It should be noted that the nuclear quantum effect can make ~ 1 kcal/mol difference in the liquid-state interaction energy[63–65] but this was not taken into account here.

4. Dielectric and dynamic properties

We evaluate the optical and static dielectric constants, relaxation times of dipole moments, and the diffusion constant of the PRG and PFG models. The optical dielectric constant ε_∞ is calculated from the expression[66]

$$\varepsilon_\infty = 1 + \frac{4\pi}{3V}\mathrm{Tr}\,\mathsf{A}\ , \tag{5.1}$$

where V is the volume of the system, A is the total polarizability tensor of the system and $\mathrm{Tr}\,\mathsf{A}$ is the trace of A. The tensor A is obtained by applying a uniform electric field of small but finite intensity to the system and evaluating the linear response of the system dipole moment to the field (finite field method). The results of 1.41 for the PRG and 1.32 for the PFG model [Table IV] is lower than the experimental value of 1.79. This underestimation of ε_∞ occurs mainly because the out-of-plane polarizability component is not included in the models. There is an additional contribution for the PFG model arising from reduced electronic polarizability. For reference, we note that this result changes a little if we use the sum of the gas-phase molecular polarizability in place of $\mathrm{Tr}\,\mathsf{A}$: 1.42 and 1.31 for the PRG and PFG models, respectively. Even though the changes are small, we observe a distinctive reduction of polarizability in liquid for the PRG model. For the PFG model, the slight increase in ε_∞ with the finite field method indicates the increase in electronic polarizability due to the change in geometry [Appendix C]. In passing, we mention that the use of Clausius-Mossotti equation[67] instead of Eq. (5.1) would yield a higher value of ε_∞ (1.47 for PRG and 1.36 for PFG).

The static dielectric constant ε_0 is obtained from the fluctuation of the system total dipole moment $\mathbf{M}$ $(= \sum_i \boldsymbol{\mu}_i)$,[66]

$$\varepsilon_0 = \varepsilon_\infty + \frac{4\pi}{3Vk_\mathrm{B}T}\langle \mathbf{M}^2 \rangle\ , \tag{5.2}$$

where k_B is Boltzmann constant and the angular brackets denote an equilibrium average. The average $\langle \mathbf{M}^2 \rangle$ was calculated from a 2 ns trajectory for each model. The standard deviation was evaluated from averages over 400 ps blocks of the total trajectory. The result given in Table IV shows that the iteration and ext-L integration method yield identical

results within the standard deviation. If the total average is taken over the entire trajectory combining the iteration and ext-L results, we find $\varepsilon_0 = 99 \pm 6$ for the PRG and 99 ± 8 for the PFG model. This is about 25 % higher than the experimental value of 78, but it should be noted that this is near optimal result within the framework of the current model. We discuss the possible reasons for the overestimation of ε_0 and ways to improve it in Section VI.

In order to further study dielectric relaxation behavior of the models, we have calculated the effective relaxation times $\tau_{\rm s}^{\rm eff}$ and $\tau_{\rm D}^{\rm eff}$ of the single-molecule and total-system dipole moment time correlation functions (TCF), $C_\mu(t)$ and $C_M(t)$, where

$$\begin{aligned} C_\mu(t) &= \langle \boldsymbol{\mu}_i(t) \cdot \boldsymbol{\mu}_i(0) \rangle \ , \\ C_M(t) &= \langle \mathbf{M}(t) \cdot \mathbf{M}(0) \rangle \ . \end{aligned} \tag{5.3}$$

Here, $\tau_{\rm s}^{\rm eff}$ and $\tau_{\rm D}^{\rm eff}$ are time constants of the long time exponential decay of $C_\mu(t)$ and $C_M(t)$, respectively. Since the actual decay of the TCFs is not a perfect exponential, $\tau_{\rm s}^{\rm eff}$ and $\tau_{\rm D}^{\rm eff}$ are slightly larger than the corresponding correlation times obtained by integrating $C_\mu(t)$ and $C_M(t)$ from $t = 0$ to ∞. However, the difference between the effective relaxation time and the correlation time was less than 10 % for the models studied here and we consider only $\tau_{\rm s}^{\rm eff}$ and $\tau_{\rm D}^{\rm eff}$. From Table IV, after averaging the iteration and ext-L results, it is found that $\tau_{\rm s}^{\rm eff} \sim 5.1$ ps and $\tau_{\rm D}^{\rm eff} \sim 11.6$ ps. Remarkably, these dipole relaxation times are essentially identical to the SPC/F values. They are also in line with the values for nonpolarizable, rigid SPC and SPC/E models: $\tau_{\rm s} = 3.3 \pm 0.2$ (SPC) and 5.3 ± 0.3 (SPC/E),[68] $\tau_{\rm D} = 11 \pm 2$ (SPC)[68] and 10 ± 3 (SPC/E).[69] The value of $\tau_{\rm D}$ for these models are somewhat higher than the experimental value of 7.9 ps.

The translational self-diffusion constant D has been used in many water modeling studies as a representative dynamical property. We calculated D from the slope of the mean square displacement,

$$D = \lim_{t \to \infty} \frac{1}{6t} \langle |\mathbf{r}_i^{\rm CM}(t) - \mathbf{r}_i^{\rm CM}(0)|^2 \rangle \ , \tag{5.4}$$

where $\mathbf{r}_i^{\rm CM}$ is the center-of-mass position of molecule i and angular brackets denote an equilibrium average. The slope was obtained from a segment between 2 and 20 ps in the mean square displacement. The values reported in Table IV were obtained by taking average and standard deviation from multiple blocks each of which are at least 50 ps long. The value of D is one of the target properties in the parameterization of the PRG and PFG models.

The resulting values of 2.42 (PRG) and 2.29×10^{-9} m^2/s (PFG) are in excellent agreement with the experimental value of 2.4×10^{-9} m^2/s at 300 K. We note that the ext-L method produces D identical to the iteration result within the standard deviation.

5. Infrared absorption

The infrared (IR) absorption coefficient $\alpha(\omega)$ is given by[70]

$$\alpha(\omega) = \frac{2\pi\omega}{3\hbar cnV}(1 - e^{-\beta\hbar\omega}) \int_{-\infty}^{\infty} dt\, e^{-i\omega t} C_M(t) \ , \tag{5.5}$$

where $\hbar$ is Planck constant divided by 2π, c is the speed of light, n is the real part of the medium refractive index and $C_M(t)$ is given in Eq. (5.3). Since this expression does not satisfy the detailed balance condition,[71,72] we multiply by the desymmetrizing factor of $2/(1 + e^{-\beta\hbar\omega})$ to obtain

$$\alpha(\omega)n(\omega) = \frac{4\pi\omega}{3\hbar cV} \tanh\left(\frac{\beta\hbar\omega}{2}\right) \int_{-\infty}^{\infty} dt\, e^{-i\omega t} C_M(t) \ . \tag{5.6}$$

This choice of quantum correction is not unique and different methods result in large differences in the corrected spectrum. The correction chosen here is a very weak one and has been employed in previous studies on far IR spectrum of water.[11,26,73,74] Due to a large uncertainty associated with the amplitude of the corrected spectra in the high frequency region, we present the intermolecular spectrum in the far IR region [Fig. 5] and consider only the peak positions at higher frequency [Table V].

The experimental IR spectrum[75] in Fig. 5 shows two distinct peaks near 180 and 620 cm^{-1}, generally associated with hindered translation and libration (hindered rotation), respectively.[2] The PRG and PFG models produce very similar spectrum in this frequency region. The librational peak is well reproduced with these models, although its position is higher at $\sim$ 750 cm^{-1} compared to experimental and SPC/F spectra. The distinct shoulder near 250 cm^{-1} matches the experimental 180 cm^{-1} peak. This shoulder is absent in the SPC/F spectrum, in line with previous studies that have shown that this translational band originates from induced dipole correlation[26,73] associated with hydrogen-bonding antisymmetric stretching.[74] Turning to the intramolecular region, we find from Table V that the blue shift of the intramolecular bending mode and the red shift of the stretching modes are well reproduced by the PFG model. There still exists a sizable discrepancy in the peak

positions. We attribute this, in part, to the neglect of anharmonicity in the intramolecular potential of PFG, which is mainly responsible for the large red shift in the OH stretching modes,[37,76] and the uncertainties related to geometry change in liquid. Specifically, a more correct accounting of the geometry dependence of charge distribution, as well as a more refined intramolecular potential function, is required for a quantitative reproduction of intramolecular IR spectrum. A quantization of the anharmonic vibrational modes may also be required to properly capture the vibrational red shifts and absorption intensities.

VI. DISCUSSION AND CONCLUDING REMARKS

We have developed a three-site polarizable and flexible water model (PFG) by employing the effective quantum mechanical description (MS-EVB) for electronic polarizability and a diffuse Gaussian charge distribution for atomic interaction sites. In order to investigate the effect of the flexibility, the rigid PRG model was also developed. As was seen in the previous section, the liquid properties of the two models are very close in most cases. Since they share a similar liquid geometry and interaction energy, we conclude that the effect of flexibility is not significant for the liquid properties investigated in this study as long as molecular geometry and electric properties are kept close *in liquid* between the rigid and flexible models. The only exception is properties directly related to intramolecular degrees of freedom, such as heat capacity and vibrational spectrum. This conclusion is in accord with many previous studies on the role of flexibility using nonpolarizable models.[77–79]

The present models produce liquid properties in generally good agreement with experiment. They show good peak positions in the radial distribution functions and the coordination number closely matches experimental data. The liquid-state interaction energy and diffusion constant also agree well with experiment. The high dielectric constant and relaxation time for the collective dipole moment are correctly exhibited. The intermolecular dynamics, as determined by the far IR spectrum, and the influence of the medium on the intramolecular vibration, are also captured by the models.

The geometry of the flexible PFG model undergoes a large change in liquid: the OH bond length increases by 2 % and the HOH bond angle decreases from 112° to 107.4°. The change in the HOH bond angle, in particular, is at odds with experiment and has a far-reaching effect on the liquid properties. As shown in Appendix C, it leads to a large increase in

molecular dipole moment both directly and indirectly by enhancing the electronic polarizability. The resulting increase in electrostatic interaction affects most properties studied here significantly. Moreover, the molecular quadrupole moment, already underestimated by the limitation of the 3-site modeling, decreases even further as a result of smaller HOH angle. This problem was handled in two ways in the current study. First, the gas-phase electronic polarizability components were adjusted individually in order to counterbalance the atomic polarization effect. As a result, the total polarizability (electronic plus atomic) of the PFG molecule in liquid is comparable to that of the PRG molecule and the average dipole moments of the two models in liquid are similar. Second, the equilibrium HOH angle was increased to 112° so that its value in liquid is in line with experimental data. While this provides a reasonable solution with good liquid properties, we plan to pursue a more fundamental remedy[6,10,34] by incorporating the geometry dependence into the charge distribution of the EVB basis states.

During the parameterization of the PFG model, it was observed that the anisotropy in the input electronic polarizability tensor $\boldsymbol{\alpha}^0$ has a large influence on the calculated properties. For example, when α^0_{zz} was varied from 55 % to 75 % of the experimental value while the trace of $\boldsymbol{\alpha}^0$ and other parameters are kept constant, the average molecular dipole moment increased by 0.18 D and the potential energy per molecule decreased by 1.6 kcal/mol, leading to stronger interactions. There was also a large impact on the dielectric constant and diffusion constant: 25 % increase in ε_0 and 36 % decrease in D were observed in going from 65 % of experimental α^0_{zz} to 75 %. If α^0_{zz} is fixed and α^0_{yy} is increased, the interaction gets stronger due to higher induced dipole moment but the diffusion constant gets *larger* and the O-O RDF exhibits softer peaks, indicating the weaking of hydrogen bonding structure. The larger transverse component α^0_{yy} weakens the structure and enhances the dynamics significantly. This indicates that the out-of-plane polarizability, ignored in this study due to the limitation of the 3-site model, would also have a large effect in the same direction. Since the PFG model exhibits a slightly stronger interaction and overestimates the dielectric constant, it is possible that the inclusion of out-of-plane polarizability component could lead to a further improvement of the model. This issue will be investigated in future work.

We have implemented the ext-L algorithm for the integration of the polarization degrees of freedom. This algorithm exhibited very good efficiency and the calculated static and dynamic properties are essentially identical to the iteration results. This demonstrates that

the ext-L algorithm can be a viable alternative to the iteration for the system studied here. Another way to check the accuracy of the ext-L method is via the deviation of the ext-L solution from the MS-EVB Schrödinger equation (Eq. (2.10)) given by

$$\Delta = 1 - \bar{h} \; ; \quad h = N_h |\langle \psi^i_{\rm eL} | \hat{h}^i_{\rm eff} | \psi^i_{\rm eL} \rangle| \; , \tag{6.1}$$

where $\psi^i_{\rm eL}$ is the electronic ground-state wavefunction obtained from the ext-L method, $N_h \equiv [\langle \psi^i_{\rm eL} | (\hat{h}^i_{\rm eff})^\dagger \hat{h}^i_{\rm eff} | \psi^i_{\rm eL} \rangle]^{-1/2}$ is the normalization constant, $\bar{h}$ is the average of h over the molecules, and $\hat{h}^i_{\rm eff}$ in these expressions should be constructed from the charge distribution of the ext-L simulation. The quantity Δ is 0 if $\psi^i_{\rm eL}$ is the exact solution to the MS-EVB Schrödinger equation and greater than 0 otherwise. From Fig. 6, we see an initial jump in Δ from 0 due to the jump in wavefunction velocity from 0. Following this, the PRG curve remains constant but the PFG curve shows a gradual increase in Δ. This shows that the ext-L method works better with the PRG model than with the PFG, which can also be inferred from the length of trajectory that can be generated without interruption (400 ps vs. 200 ps, Section IV). However, the magnitude of error is very small even for the PFG model and the wavefunction from the ext-L method remains a very good approximation to the exact solution after 100 ps. This result is important because the ext-L approach is considerably more efficient than the iteration method for these models.

Future research will focus on generalizations of the present model to treat more elaborate charge distributions, more accurate intramolecular potentials, and a correct description of the effects of molecular vibrations on the permanent and induced dipoles.

Acknowledgments

This research was supported by a grant through the Department of Energy Solar Photochemistry Program, Office of Basic Energy Sciences.

APPENDIX A: LONG-RANGE ELECTROSTATIC INTERACTIONS IN THE GCD MODEL

In this study, the long-range electrostatic interaction is treated by the Ewald sum method. As is shown in Section III, optimal values of the GCD width ξ_α are less than 1 Å. Since the

width of the Gaussian screening charge ξ_s employed in the Ewald sum for the point charge distribution is usually $\gtrsim 2$ Å, we can apply the same standard Ewald sum technique with the Gaussian screening charge distribution to the GCD case. In this case, the standard Ewald expression for point charge distribution should be modified based on Eq. (2.13). The Coulombic interaction operator $\hat{H}_{\rm Coul}$ in Eq. (2.8) should then be replaced by $\hat{H}_{\rm Coul}^{\rm Ewald}$,

$$\hat{H}_{\rm Coul}^{\rm Ewald} = \hat{H}_{\rm Coul}^{\rm RS} + \hat{H}_{\rm Coul}^{\rm KS} + \hat{H}_{\rm Coul}^{\rm self} \; ; \tag{A1}$$

$$\hat{H}_{\rm Coul}^{\rm RS} = \frac{1}{2}\sum_{i=1}^{N}\sum_{\alpha}\sum_{\substack{j=1\\(j\neq i)}}^{N}\sum_{\beta}\frac{\hat{q}_{i\alpha}\hat{q}_{j\beta}}{r_{i\alpha,j\beta}}\left[\mathrm{erf}(\kappa_{\alpha\beta}r_{i\alpha,j\beta}) - \frac{1}{2}\mathrm{erf}(\kappa_{\alpha s}r_{i\alpha,j\beta}) - \frac{1}{2}\mathrm{erf}(\kappa_{\beta s}r_{i\alpha,j\beta})\right] \; ,$$

$$\hat{H}_{\rm Coul}^{\rm KS} = \frac{\pi}{L^3}\sum_{i=1}^{N}\sum_{\alpha}\sum_{j=1}^{N}\sum_{\beta}\sum_{\mathbf{k}\neq\mathbf{0}}\frac{\hat{q}_{i\alpha}\hat{q}_{j\beta}}{k^2}\cos(\mathbf{k}\cdot\mathbf{r}_{i\alpha,j\beta})\left[\exp\left(-\frac{k^2}{4\kappa_{\alpha s}^2}\right) + \exp\left(-\frac{k^2}{4\kappa_{\beta s}^2}\right)\right] \; ,$$

$$\hat{H}_{\rm Coul}^{\rm self} = -\frac{1}{\sqrt{\pi}}\sum_{i=1}^{N}\sum_{\alpha}\kappa_{\alpha s}\hat{q}_{i\alpha}\hat{q}_{i\alpha} - \frac{1}{4}\sum_{i=1}^{N}\sum_{\alpha}\sum_{\beta(\neq\alpha)}\frac{\hat{q}_{i\alpha}\hat{q}_{i\beta}}{r_{i\alpha,i\beta}}\left[\mathrm{erf}(\kappa_{\alpha s}r_{i\alpha,i\beta}) + \mathrm{erf}(\kappa_{\beta s}r_{i\alpha,i\beta})\right] \; ,$$

where $\kappa_{\alpha\beta}$ and $\kappa_{\alpha s}$ are defined by

$$\kappa_{\alpha\beta} = \frac{1}{\sqrt{2(\xi_\alpha^2+\xi_\beta^2)}} \; , \qquad \kappa_{\alpha s} = \frac{1}{\sqrt{2(\xi_\alpha^2+\xi_s^2)}} \; , \tag{A2}$$

$\mathbf{r}_{i\alpha,j\beta} = \mathbf{r}_{i\alpha} - \mathbf{r}_{j\beta}$, L is the length of the cubic simulation box, and $\mathbf{k} = (2\pi/L)(n_x, n_y, n_z)$ with n_x, n_y, n_z integers. In Eq. (A1), the three terms that constitute $\hat{H}_{\rm Coul}^{\rm Ewald}$ are the real space screened interaction, the reciprocal space screening charge interaction, and the ionic and intramolecular self-energy corrections, respectively. For convenience in the following development, they are written in a symmetrized form over $(i\alpha)$ and $(j\beta)$. It is also convenient to express $\hat{H}_{\rm Coul}^{\rm Ewald}$ as follows

$$\hat{H}_{\rm Coul}^{\rm Ewald} = \sum_{i=1}^{N}\sum_{\alpha}\sum_{j=1}^{N}\sum_{\beta}\hat{q}_{i\alpha}\hat{q}_{j\beta}G_{i\alpha,j\beta}(\mathbf{r}_{i\alpha},\mathbf{r}_{j\beta}) \; ;$$

$$\begin{aligned} G_{i\alpha,j\beta}(\mathbf{r}_{i\alpha},\mathbf{r}_{j\beta}) &= \frac{1}{2}(1-\delta_{ij})\frac{1}{r_{i\alpha,j\beta}}\left[\mathrm{erf}(\kappa_{\alpha\beta}r_{i\alpha,j\beta}) - \frac{1}{2}\mathrm{erf}(\kappa_{\alpha s}r_{i\alpha,j\beta}) - \frac{1}{2}\mathrm{erf}(\kappa_{\beta s}r_{i\alpha,j\beta})\right] \\ &+ \frac{\pi}{L^3}\sum_{\mathbf{k}\neq\mathbf{0}}\frac{\cos(\mathbf{k}\cdot\mathbf{r}_{i\alpha,j\beta})}{k^2}\left[\exp\left(-\frac{k^2}{4\kappa_{\alpha s}^2}\right) + \exp\left(-\frac{k^2}{4\kappa_{\beta s}^2}\right)\right] \\ &- \frac{1}{\sqrt{\pi}}\delta_{ij}\delta_{\alpha\beta}\kappa_{\alpha s} - \frac{1}{4}\delta_{ij}(1-\delta_{\alpha\beta})\frac{1}{r_{i\alpha,i\beta}}\left[\mathrm{erf}(\kappa_{\alpha s}r_{i\alpha,i\beta}) + \mathrm{erf}(\kappa_{\beta s}r_{i\alpha,i\beta})\right] \; . \end{aligned} \tag{A3}$$

The effective molecular Hamiltonian operator $\hat{h}_{\rm eff}^i$ and the system total energy E can be obtained in a straightforward way by substituting Eq. (A3) for the Coulombic terms in

Eqs. (2.10) and (2.11) and then replacing the charge operators with the corresponding expectation values as the original expressions indicate. For example, $\hat{h}^i_{\rm eff}$ is given as

$$\hat{h}^i_{\rm eff} = \hat{h}^0_i + 2\sum_{\alpha}\sum_{j=1}^{N}\sum_{\beta} q_{j\beta}\hat{q}_{i\alpha}G_{i\alpha,j\beta}(\mathbf{r}_{i\alpha},\mathbf{r}_{j\beta}) \ , \tag{A4}$$

where $q_{i\alpha} = \langle\psi^i|\hat{q}_{i\alpha}|\psi^i\rangle$. We also introduce the effective electric potential $\Phi_{i\alpha}(\mathbf{r}_{i\alpha})$ at the atomic site α of molecule i,

$$\Phi_{i\alpha}(\mathbf{r}_{i\alpha}) \equiv \frac{\partial E}{\partial q_{i\alpha}} = 2\sum_{j=1}^{N}\sum_{\beta} q_{j\beta}G_{i\alpha,j\beta}(\mathbf{r}_{i\alpha},\mathbf{r}_{j\beta}) \ . \tag{A5}$$

The system Coulombic energy $E_{\rm Coul}$ is related to $\Phi_{i\alpha}(\mathbf{r}_{i\alpha})$ by the familiar relation

$$E_{\rm Coul} \equiv \langle\Psi|\hat{H}^{\rm Ewald}_{\rm Coul}|\Psi\rangle = \frac{1}{2}\sum_{i=1}^{N}\sum_{\alpha} q_{i\alpha}\Phi_{i\alpha}(\mathbf{r}_{i\alpha}) \ . \tag{A6}$$

APPENDIX B: DETAILS OF THE EXTENDED LAGRANGIAN ALGORITHM FOR THE MS-EVB MOLECULAR DYNAMICS

In the velocity Verlet algorithm, the EVB coefficients at time $t+\delta t$ and the coefficient velocities at time $t+(1/2)\delta t$ are first determined from the values at time t based on Eq. (2.18) without the normalization constraints

$$\begin{aligned}
\tilde{c}^i_n(t+\delta t) &= c^i_n(t) + \delta t\dot{c}^i_n(t) - \frac{\delta t^2}{m_c}\sum_m c^i_m(t)(\hat{h}^i_{\rm eff})_{mn} \ , \\
\dot{\tilde{c}}^i_n(t+\frac{1}{2}\delta t) &= \dot{c}^i_n(t) - \frac{\delta t}{m_c}\sum_m c^i_m(t)(\hat{h}^i_{\rm eff})_{mn} \ .
\end{aligned} \tag{B1}$$

Then, we apply the constraint force to obtain a formal expression for the corrected coefficients at time $t+\delta t$

$$c^i_n(t+\delta t) = \tilde{c}^i_n(t+\delta t) + \frac{\delta t^2}{m_c}\Lambda_i c^i_n(t) \ . \tag{B2}$$

Imposing the normalization condition to $c^i_n(t+\delta t)$, we obtain the equation for Λ_i

$$\frac{\delta t^4}{m_c^2}\left[\sum_n |c^i_n(t)|^2\right]\Lambda_i^2 + 2\frac{\delta t^2}{m_c}\left[\sum_n \tilde{c}^i_n(t+\delta t)c^i_n(t)\right]\Lambda_i + \sum_n |\tilde{c}^i_n(t+\delta t)|^2 = 1 \ . \tag{B3}$$

The multiplier Λ_i is given as the larger of the two possible solutions to this quadratic equation. This Λ_i is then used in Eq. (B2) to complete the specification of $c^i_n(t+\delta t)$. The

same Λ_i is also used to update the coefficient velocities

$$\dot{\tilde{c}}_n^i(t+\delta t) = \dot{\tilde{c}}_n^i(t+\frac{1}{2}\delta t) - \frac{\delta t}{m_c}\sum_m c_m^i(t+\delta t)(\hat{h}_{\rm eff}^i)_{mn}(t+\delta t) + \frac{\delta t}{m_c}\Lambda_i c_n^i(t) \ , \tag{B4}$$

where $(\hat{h}_{\rm eff}^i)_{mn}(t+\delta t) = \langle m|\hat{h}_{\rm eff}^i(t+\delta t)|n\rangle$ determined with $c_n^i(t+\delta t)$'s in Eq. (B2). The final coefficient velocities at time $t+\delta t$ are written as

$$\dot{c}_n^i(t+\delta t) = \dot{\tilde{c}}_n^i(t+\delta t) + \Gamma_i c_n^i(t+\delta t) \ , \tag{B5}$$

where the last term involving Γ_i is the correction to satisfy the following relation obtained by taking time derivative of the coefficient normalization condition at time $t+\delta t$

$$\sum_n \dot{c}_n^i(t+\delta t)c_n^i(t+\delta t) = 0 \ . \tag{B6}$$

Using Eqs. (B5) and (B6), Γ_i is determined as

$$\Gamma_i = -\sum_n \dot{\tilde{c}}_n^i(t+\delta t)c_n^i(t+\delta t) \ . \tag{B7}$$

This Γ_i is then used in Eq. (B5) to complete the coefficient velocities at $t+\delta t$.

The algorithm described above can be inserted in the standard velocity Verlet integration scheme in the following order:

1. Given the positions $\{\mathbf{r}_{i\alpha}(t)\}$ and velocities $\{\dot{\mathbf{r}}_{i\alpha}(t)\}$, the first stage of the standard velocity Verlet algorithm is carried out, yielding $\{\mathbf{r}_{i\alpha}(t+\delta t)\}$ and $\{\dot{\mathbf{r}}_{i\alpha}(t+(1/2)\delta t)\}$.

2. Given $\{c_n^i(t)\}$ and $\{\dot{c}_n^i(t)\}$, $\{c_n^i(t+\delta t)\}$ and $\{\dot{c}_n^i(t+(1/2)\delta t)\}$ are obtained from Eqs. (B1), (B2), and (B3).

3. Forces for nuclear degrees freedom are calculated at time $t+\delta t$ based on $\{\mathbf{r}_{i\alpha}(t+\delta t)\}$ and the updated charge distribution from $\{c_n^i(t+\delta t)\}$.

4. The velocities $\{\dot{\mathbf{r}}_{i\alpha}(t+\delta t)\}$ are calculated from the forces just obtained (second stage of the standard velocity Verlet).

5. The time derivatives $\{\dot{c}_n^i(t+\delta t)\}$ are obtained from Eqs. (B4), (B5), and (B7).

6. The above procedure is repeated for the next time step $t+2\delta t$.

When a rigid potential is used, the standard RATTLE algorithm for the bond constraints[41] can be added to the first and fourth steps in the above procedure.

APPENDIX C: EFFECT OF MOLECULAR DEFORMATION ON THE POLARIZABILITY OF A PFG WATER MOLECULE

In Section II A, we have developed the single-molecule electronic Hamiltonian in the EVB basis, $h^0_{\rm EVB}$, based on the equilibrium geometry of the molecule. While this is exact for the rigid PRG model, it ignores the intramolecular deformation of the flexible PFG model. Since we observed a significant geometry change for the PFG water in liquid [Section V B 1], its electronic polarizability will be different from its gas-phase value. We can evaluate this modified polarizability by (i) taking a single PFG molecule from the liquid with its geometry fixed at its average liquid value and (ii) applying Eq. (2.6) for $\boldsymbol{\alpha}$. Here, we note that the eigenvalues and eigenfunctions entering the expression for $\boldsymbol{\alpha}$ are the same as in the molecule with gas-phase equilibrium geometry since $h^0_{\rm EVB}$ is the same. The only difference is in the dipole operator $\hat{\boldsymbol{\mu}}$ due to the change in molecular geometry. Using the average liquid-phase geometry of a PFG molecule from Table IV, we obtain $\alpha_{yy} = 1.2819$ Å^3 and $\alpha_{zz} = 1.1130$ Å^3. This is a 1 % decrease from the gas-phase value for α_{yy} and 17 % increase for α_{zz}. Compared to the experimental polarizability, α_{yy} and α_{zz} for a liquid-phase molecule are 84 and 76 % of the corresponding experimental value. The electronic polarizability of a PFG molecule becomes nearly isotropic in liquid as a result of the anisotropic change from the gas-phase value.

In addition to this electronic effect, the deformation of a PFG molecule enhances the molecular dipole moment through the change in geometry itself (atomic polarization, Ref. 67). It is less straightforward to calculate this atomic polarizability. However, we can estimate its magnitude using a reaction field argument. We first recall the following expressions involving the reaction field $\mathbf{R}$ of a polar polarizable dipole[67]

$$\begin{aligned} R &= \frac{f}{1 - f\bar{\alpha}}\,\mu_{\rm pe}\ , \\ \mu_{\rm ind} &= \bar{\alpha} R\ , \end{aligned} \tag{C1}$$

where f is the reaction field factor given by $f = 2(\varepsilon_0 - 1)/[(2\varepsilon_0 + 1)a^3]$ with a the radius of the spherical cavity accommodating the dipole, $\bar{\alpha} \equiv {\rm Tr}\,\boldsymbol{\alpha}/3$ is the isotropic polarizability of the dipole, $\mu_{\rm pe}$ and $\mu_{\rm ind}$ are the permanent and induced part of the dipole, and we consider only scalar quantities since all the vector quantities are in the same direction. The cavity radius a will be similar for the PRG and PFG molecule since they have a similar geometry in

the liquid. Therefore, we use $a = 1.513$ Å obtained from the above expression using data for the PRG model. With this value for a, $\bar{\alpha}$ for the PFG molecule is found to be 1.01 Å^3. Since the electronic contribution $\bar{\alpha}_{\rm el}$ to this is $(1.2819 + 1.1130)/3 = 0.80$ Å^3 from the previous paragraph, we find the atomic polarizability $\bar{\alpha}_{\rm at}$ to be 0.21 Å^3. The atomic polarization is thus responsible for about 20 % of the total polarization of the PFG molecule in liquid.

---

[1] A. Wallqvist and R. D. Mountain, Rev. Comp. Chem. **13**, 183 (1999).

[2] D. Eisenberg and W. Kauzmann, *The structure and properties of water* (Oxford, New York, 1969).

[3] S. W. Rick and S. J. Stuart, Rev. Comp. Chem. **18**, 89 (2002).

[4] F. H. Stillinger and C. W. David, J. Chem. Phys. **69**, 1473 (1978).

[5] G. King and A. Warshel, J. Chem. Phys. **91**, 3647 (1989).

[6] A. Wallqvist, Chem. Phys. **148**, 439 (1990).

[7] S.-B. Zhu, S. Singh, and G. W. Robinson, J. Chem. Phys. **95**, 2791 (1991).

[8] G. Corongiu, Int. J. Quantum Chem. **42**, 1209 (1992).

[9] H. Saint-Martin, J. Hernández-Cobos, M. I. Bernal-Uruchurtu, I. Ortega-Blake, and H. J. C. Berendsen, J. Chem. Phys. **113**, 10899 (2000).

[10] C. J. Burnham and S. S. Xantheas, J. Chem. Phys. **116**, 5115 (2002).

[11] S. Iuchi, A. Morita, and S. Kato, J. Phys. Chem. B **106**, 3466 (2002).

[12] P. Ren and J. W. Ponder, J. Chem. Phys. (to be published).

[13] A. Warshel and R. M. Weiss, J. Am. Chem. Soc. **102**, 6218 (1980).

[14] R. Vuilleumier and D. Borgis, Chem. Phys. Lett. **284**, 71 (1998).

[15] U. W. Schmitt and G. A. Voth, J. Phys. Chem. B **102**, 5547 (1998).

[16] U. W. Schmitt and G. A. Voth, J. Chem. Phys. **111**, 9361 (1999).

[17] T. J. F. Day, A. V. Soudackov, M. . Cuma, U. W. Schmitt, and G. A. Voth, J. Chem. Phys. **117**, 5839 (2002).

[18] A. Warshel, J. Phys. Chem. **86**, 2218 (1982).

[19] J. Åqvist and A. Warshel, Chem. Rev. **93**, 2523 (1993).

[20] A. E. Lefohn, M. Ovchinnikov, and G. A. Voth, J. Phys. Chem. B **105**, 6628 (2001).

[21] N. S. Bayliss, J. Chem. Phys. **18**, 292 (1950).

[22] A. Warshel, J. Phys. Chem. **83**, 1640 (1979).

[23] B. D. Bursulaya and H. J. Kim, J. Chem. Phys. **108**, 3277 (1998).

[24] B. D. Bursulaya, J. Jeon, D. A. Zichi, and H. J. Kim, J. Chem. Phys. **108**, 3286 (1998).

[25] B. D. Bursulaya, J. Jeon, C.-N. Yang, and H. J. Kim, J. Phys. Chem. A **104**, 45 (2000).

[26] B. D. Bursulaya and H. J. Kim, J. Chem. Phys. **109**, 4911 (1998).

[27] R. Car and M. Parrinello, Phys. Rev. Lett. **55**, 2471 (1985).

[28] H. B. Schlegel, J. M. Millam, S. S. Iyengar, G. A. Voth, A. D. Daniels, G. E. Scuseria, and M. J. Frisch, J. Chem. Phys. **114**, 9758 (2001).

[29] M. Sprik and M. L. Klein, J. Chem. Phys. **89**, 7556 (1988).

[30] S. W. Rick, S. J. Stuart, and B. J. Berne, J. Chem. Phys. **101**, 6141 (1994).

[31] A. A. Chialvo and P. T. Cummings, Fluid Phase Equilib. **150-151**, 73 (1998).

[32] U. Dinur, J. Phys. Chem. **94**, 5669 (1990).

[33] W. E. Thiessen and A. H. Narten, J. Chem. Phys. **77**, 2656 (1982).

[34] M. A. Suhm and R. O. Watts, Mol. Phys. **73**, 463 (1991).

[35] D. Borgis and A. Staib, Chem. Phys. Lett. **238**, 187 (1995).

[36] A. Szabo and N. S. Ostlund, *Modern Quantum Chemistry: Introduction to Advanced Electronic Structure Theory* (McGraw-Hill, New York, 1982).

[37] K. Toukan and A. Rahman, Phys. Rev. B **31**, 2643 (1985).

[38] H. C. Andersen, J. Chem. Phys. **72**, 2384 (1980).

[39] S. Nosé, Mol. Phys. **52**, 255 (1984).

[40] M. E. Tuckerman and M. Parrinello, J. Chem. Phys. **101**, 1302 (1994).

[41] M. P. Allen and D. J. Tildesley, *Computer Simulation of Liquids* (Oxford, Oxford, 1987).

[42] H. J. C. Berendsen, J. P. M. Postma, W. F. van Gunsteren, and J. Hermans, in *Intermolecular Forces*, edited by B. Pullman (Reidel, Dordrecht, 1981), p. 331.

[43] S. A. Clough, Y. Beers, and G. P. Klein, J. Chem. Phys. **59**, 2254 (1973).

[44] W. F. Murphy, J. Chem. Phys. **67**, 5877 (1977).

[45] C. J. Burnham, J. Li, S. S. Xantheas, and M. Leslie, J. Chem. Phys. **110**, 4566 (1999).

[46] W. S. Benedict, N. Gailar, and E. K. Plyler, J. Chem. Phys. **24**, 1139 (1956).

[47] K. Kuchitsu and Y. Morino, Bull. Chem. Soc. Japan **38**, 814 (1965).

[48] M. Sprik, M. L. Klein, and K. Watanabe, J. Phys. Chem. **94**, 6483 (1990).

[49] G. G. Hall and C. M. Smith, Int. J. Quantum Chem. **42**, 1237 (1992).

[50] W. L. Jorgensen, J. Chandrasekhar, J. D. Madura, R. W. Impey, and M. L. Klein, J. Chem. Phys. **79**, 926 (1983).

[51] B. Chen, J. Xing, and J. I. Siepmann, J. Phys. Chem. B **104**, 2391 (2000).

[52] M. W. Mahoney and W. L. Jorgensen, J. Chem. Phys. **112**, 8910 (2000).

[53] K. Ichikawa, Y. Kameda, T. Yamaguchi, and H. Wakita, Mol. Phys. **73**, 79 (1991).

[54] N. W. Moriarty and G. Karlström, J. Chem. Phys. **106**, 6470 (1997).

[55] P. L. Silvestrelli and M. Parrinello, J. Chem. Phys. **111**, 3572 (1999).

[56] S. Izvekov and G. A. Voth, J. Chem. Phys. **116**, 10372 (2002).

[57] M. Sprik, J. Chem. Phys. **95**, 6762 (1991).

[58] L. X. Dang, J. Chem. Phys. **97**, 2659 (1992).

[59] I. M. Svishchev, P. G. Kusalik, J. Wang, and R. J. Boyd, J. Chem. Phys. **105**, 4742 (1996).

[60] G. G. Ferenczy and C. A. Reynolds, J. Phys. Chem. A **105**, 11470 (2001).

[61] J. M. Sorenson, G. Hura, R. M. Glaeser, and T. Head-Gordon, J. Chem. Phys. **113**, 9149 (2000).

[62] A. K. Soper, Chem. Phys. **258**, 121 (2000).

[63] J. Lobaugh and G. A. Voth, J. Chem. Phys. **106**, 2400 (1997).

[64] H. A. Stern and B. J. Berne, J. Chem. Phys. **115**, 7622 (2001).

[65] M. W. Mahoney and W. L. Jorgensen, J. Chem. Phys. **115**, 10758 (2001).

[66] M. Neumann and O. Steinhauser, Chem. Phys. Lett. **106**, 563 (1984).

[67] C. J. F. Böttcher, O. C. van Belle, P. Bordewijk, and A. Rip, *Theory of Electric Polarization*, vol. 1 (Elsevier, Amsterdam, 1973), 2nd ed.

[68] K. Watanabe and M. L. Klein, Chem. Phys. **131**, 157 (1989).

[69] D. E. Smith and L. X. Dang, J. Chem. Phys. **100**, 3757 (1994).

[70] D. A. McQuarrie, *Statistical Mechanics* (Harper & Row, New York, 1976).

[71] J. Borysow, M. Moraldi, and L. Frommhold, Mol. Phys. **56**, 913 (1985).

[72] L. Frommhold, *Collision-induced absorption in gases* (Cambridge, Cambridge, 1993).

[73] B. Guillot, J. Chem. Phys. **95**, 1543 (1991).

[74] P. L. Silvestrelli, M. Bernasconi, and M. Parrinello, Chem. Phys. Lett. **277**, 478 (1997).

[75] J. E. Bertie and Z. Lan, Appl. Spectrosc. **50**, 1047 (1996).

[76] J. R. Reimers and R. O. Watts, Chem. Phys. **91**, 201 (1984).

[77] J.-L. Barrat and I. R. McDonald, Mol. Phys. **70**, 535 (1990).

[78] D. E. Smith and A. D. J. Haymet, J. Chem. Phys. **96**, 8450 (1992).

[79] I. G. Tironi, R. M. Brunne, and W. F. van Gunsteren, Chem. Phys. Lett. **250**, 19 (1996).

[80] J. Verhoeven and A. Dymanus, J. Chem. Phys. **52**, 3222 (1970).

[81] J. A. Odutola and T. R. Dyke, J. Chem. Phys. **72**, 5062 (1980).

[82] L. A. Curtiss, D. J. Frurip, and M. Blander, J. Chem. Phys. **71**, 2703 (1979).

[83] Y. S. Badyal, M.-L. Saboungi, D. L. Price, S. D. Shastri, D. R. Haeffner, and A. K. Soper, J. Chem. Phys. **112**, 9206 (2000).

[84] W. L. Jorgensen, J. Am. Chem. Soc. **103**, 335 (1981).

[85] K. Krynicki, C. D. Green, and D. W. Sawyer, Faraday Discuss. Chem. Soc. **66**, 199 (1978).

[86] A. D. Buckingham, Proc. R. Soc. London, Ser. A **238**, 235 (1956).

[87] J. Anderson, J. J. Ullo, and S. Yip, J. Chem. Phys. **87**, 1726 (1987).

[88] U. Kaatze and V. Uhlendorf, Z. Phys. Chem. N. F. **126**, 151 (1981).

[89] J. G. Bayly, V. B. Kartha, and W. H. Stevens, Infrared Phys. **3**, 211 (1963).

TABLE I: Parameters for the rigid (PRG) and the flexible (PFG) water models with MS-EVB description of polarizability. In respective order, the parameters are defined as follows: $r^0_{\rm OH}$ and $(\angle{\rm HOH})^0$: Equilibrium OH bond length and HOH bond angle in the gas phase. μ^0, α^0_{xx}, α^0_{yy} and α^0_{zz}: Gas-phase dipole moment and polarizability components. Q^0_{xx}, Q^0_{yy} and Q^0_{zz}: Quadrupole moment derived from the geometry and dipole moment. (The molecule lies on the yz-plane with the symmetry axis z.) $\xi_{\rm O}$ and $\xi_{\rm H}$: Widths of Gaussian charge distribution for O and H atomic sites. ϵ and σ: LJ parameters between O atomic sites.

Parameter	PRG	PFG	Exp.
$r^0_{\rm OH}$ (Å)	1.0	1.0	0.9572[a]
$(\angle{\rm HOH})^0$ (°)	107.47	112.0	104.52[a]
μ^0 (D)	1.855	1.855	1.855[b]
α^0_{xx} (Å^3)	0	0	1.415[c]
α^0_{yy} (Å^3)	1.528	1.2928	1.528[c]
α^0_{zz} (Å^3)	1.468	0.9542	1.468[c]
$\xi_{\rm O}$ (Å)	0.8	0.8	-
$\xi_{\rm H}$ (Å)	0.8	0.8	-
ϵ (kcal/mol)	0.15544	0.139896	-
σ (Å)	3.165	3.215	-
Q^0_{xx} (DÅ)[d]	−1.445	−1.543	−2.5[e]
Q^0_{yy} (DÅ)[d]	1.613	1.877	2.63[e]
Q^0_{zz} (DÅ)[d]	−0.168	−0.335	−0.13[e]

[a]Ref. 46.
[b]Ref. 43.
[c]Ref. 44.
[d]Quadrupole moments are not part of the model parameters and determined from the geometry and dipole moment.
[e]Ref. 80.

TABLE II: Intramolecular potential constants and vibrational frequencies for an isolated water molecule. The entries $\omega_{\rm as}$, $\omega_{\rm s}$ and $\omega_{\rm b}$ are frequencies for asymmetric stretch, symmetric stretch and bending modes, respectively.

	PFG	Exp.
a (kcal/(mol·Å^2))	1342[a]	-
b (kcal/(mol·Å^2))	328.6[a]	-
c (kcal/(mol·Å^2))	−211.4[a]	-
d (kcal/(mol·Å^2))	111.7[a]	-
$\omega_{\rm as}$ (cm^{-1})	3978	3756[b]
$\omega_{\rm s}$ (cm^{-1})	3842	3657[b]
$\omega_{\rm b}$ (cm^{-1})	1602	1595[b]

[a]Ref. 37.
[b]Ref. 46.

TABLE III: Properties of the water dimer. [r_{OO}: the oxygen-oxygen distance. D_e: Equilibrium dissociation energy. θ_d and θ_a: Angle between the O-O axis and the symmetry axis of the hydrogen-bond donor and acceptor molecule, respectively.] Experimental uncertainties from the original literature are indicated in parentheses.

	PRG	PFG	Exp.
r_{OO} (Å)	2.76	2.80	2.98(0,-0.03)[a]
D_e (kcal/mol)	5.1	5.0	5.4(0.7)[b]
θ_d (°)	51	53	51(10)[a]
θ_a (°)	15	16	57(10)[a]

[a]Ref. 81.
[b]Ref. 82.

TABLE IV: Liquid properties of the MS-EVB water models at $T = 300$ K and $\rho = 0.997$ g/cm^3. For comparison, results for the nonpolarizable, flexible SPC/F model (Ref. 37) are also given. If the entry has two values, the first is from the iteration method and the second from the ext-L. Otherwise, the results from the two methods are identical. Numbers in parentheses are the standard deviation from the average or the experimental uncertainty.

	SPC/F	PRG	PFG	Exp.
$\bar{r}_{\mathrm{OH}}$ (Å)	1.02	1.00	1.02	0.970(0.005)[a]
$\overline{\angle \mathrm{HOH}}$ (°)	105.74	107.47	107.39	106(2)[b]
$\bar{\mu}$ (D)	2.42	2.590	2.604	2.9(0.6)[c]
V_{Intra} (kcal/mol)	1.51	-	1.79	-
V_{Inter} (kcal/mol)	−11.36	−10.02	−10.56	-
$V(l) - V(g)$ (kcal/mol)	−10.78	−10.02	−9.70	−9.92[d]
C_{v} (cal/(mol·K))	25.2	16.9, 17.0	27.2, 27.7	18[e]
D (10^{-9}m^2/s)	3.0	2.44(0.04), 2.40(0.03)	2.29(0.07), 2.28(0.04)	2.4[f]
ε_∞	1	1.41	1.32	1.79[g]
ε_0	91(10)	101(4), 98(9)	97(3), 101(11)	78[g]
$\tau_{\mathrm{s}}^{\mathrm{eff}}$ (ps)	5.0[h]	5.0(0.2), 5.2(0.1)	5.1(0.2), 5.2(0.2)	-
$\tau_{\mathrm{D}}^{\mathrm{eff}}$ (ps)	11.6(0.4)	11.3(1.2), 11.8(0.4)	11.4(1.3), 11.7(1.3)	7.9[i]

[a] Ref. 53.
[b] Calculated from intramolecular distances of Ref. 53.
[c] Ref. 83.
[d] Ref. 50.
[e] Ref. 84.
[f] Interpolation from the data of Ref. 85.
[g] Ref. 86.
[h] Reported in Ref. 87 with a variant of SPC/F employing an anharmonic intramolecular potential.
[i] Interpolation from the data of Ref. 88.

TABLE V: Peak positions of liquid water IR spectra and shifts from gas phase frequencies (in cm^{-1}). ω_L is the peak frequency of the librational band. Other frequencies have the same meaning as in Table II. $\Delta\omega = \omega(\text{liquid}) - \omega(\text{gas})$.

	SPC/F[a]	PRG[a]	PFG[a]	Exp.
ω_L	640	750	750	620[b]
ω_b	1815	-	1785	1645[c]
ω_s	3836	-	3802	3280[c]
ω_{as}	3943	-	3916	3490[c]
$\Delta\omega_b$	158	-	183	50
$\Delta\omega_s$	-5	-	-40	-377
$\Delta\omega_{as}$	-30	-	-62	-266

[a]Peak positions of the function $n(\omega)\alpha(\omega)$ (Eq. 5.6).

[b]Peak position of the librational band from the experimental $n(\omega)\alpha(\omega)$ from Ref. 75. This can be different by a few tens of cm^{-1} from peak positions determined from the absorption coefficient $\alpha(\omega)$ only.

[c]Ref. 89.

FIGURES

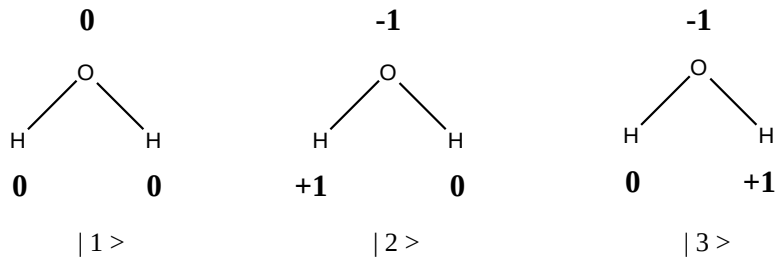

FIG. 1: EVB basis states for a water molecule. Numbers indicate charges associated with each atomic site.

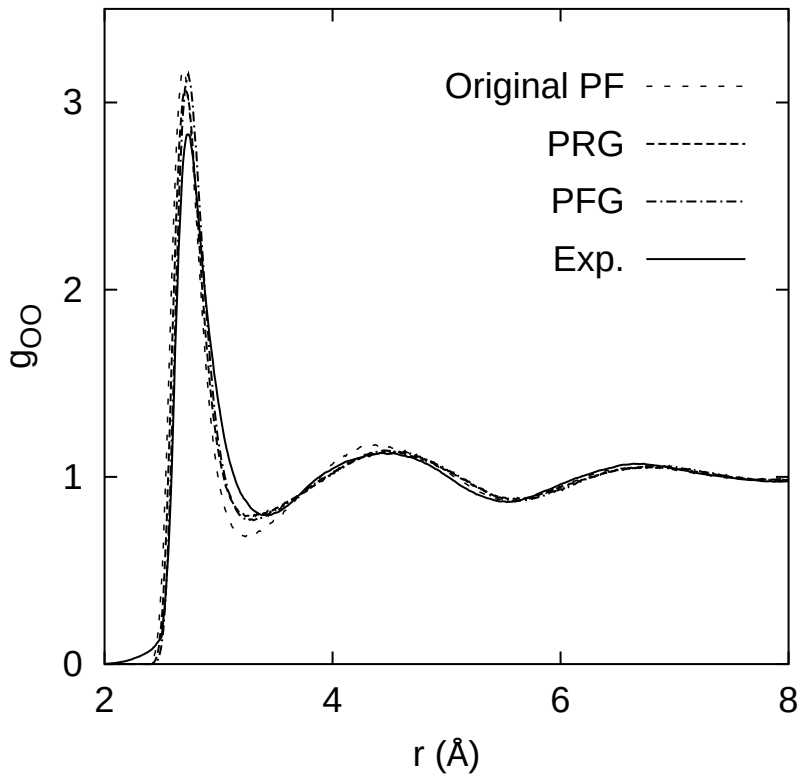

FIG. 2: O-O radial distribution function. Experimental curve is from Ref. 61.

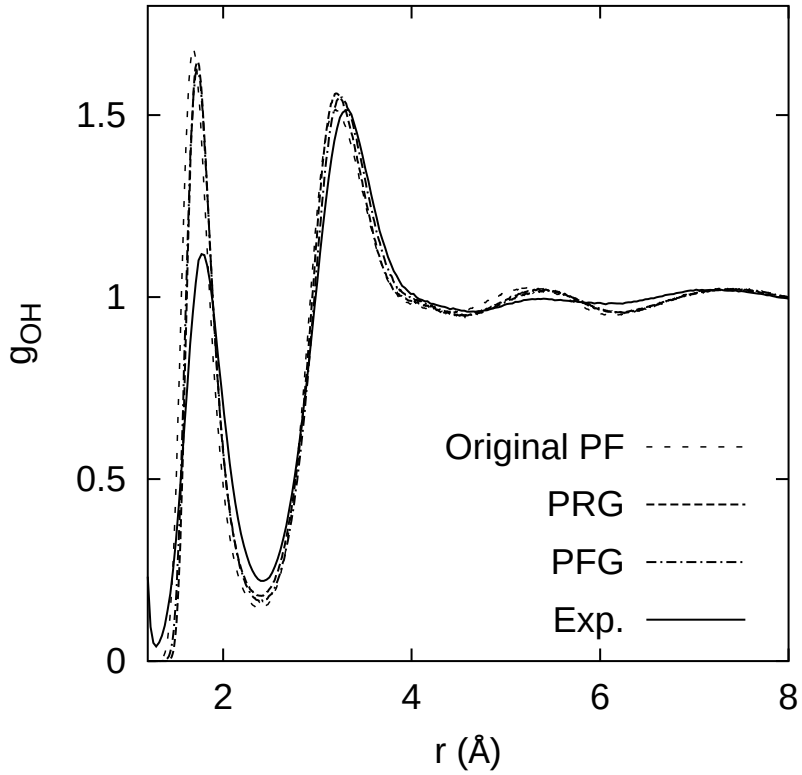

FIG. 3: O-H radial distribution function. Experimental curve is from Ref. 62.

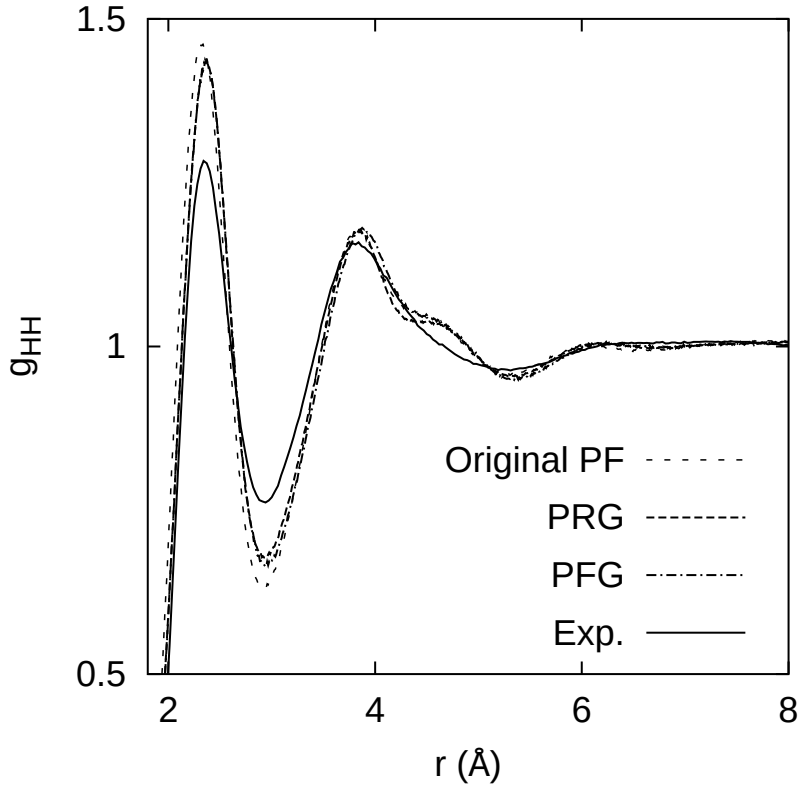

FIG. 4: H-H radial distribution function. Experimental curve is from Ref. 62.

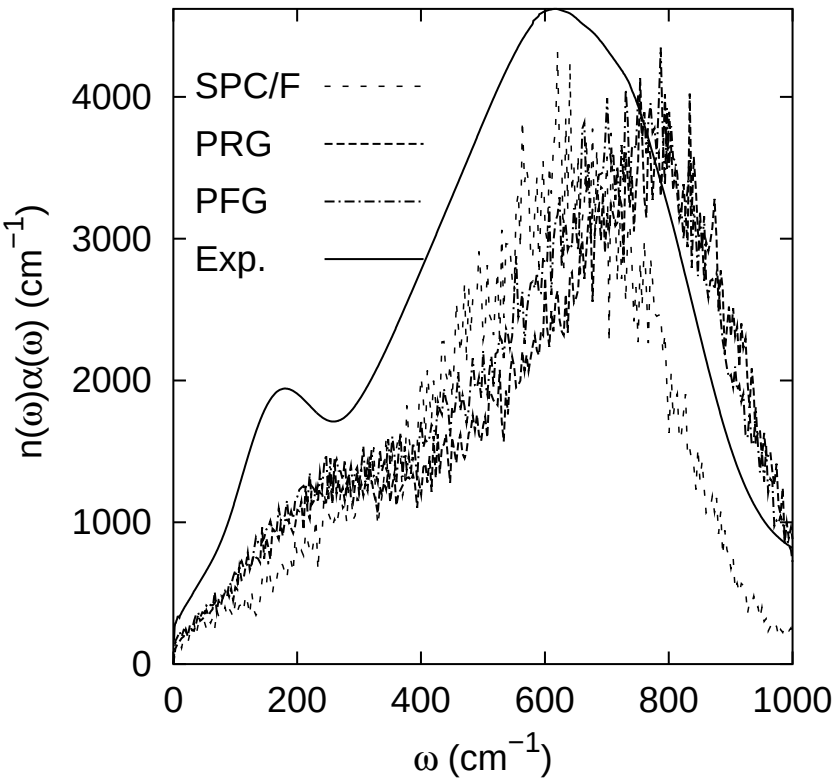

FIG. 5: Far infrared abrorption spectra of liquid water. Experimental spectrum is from Ref. 75.

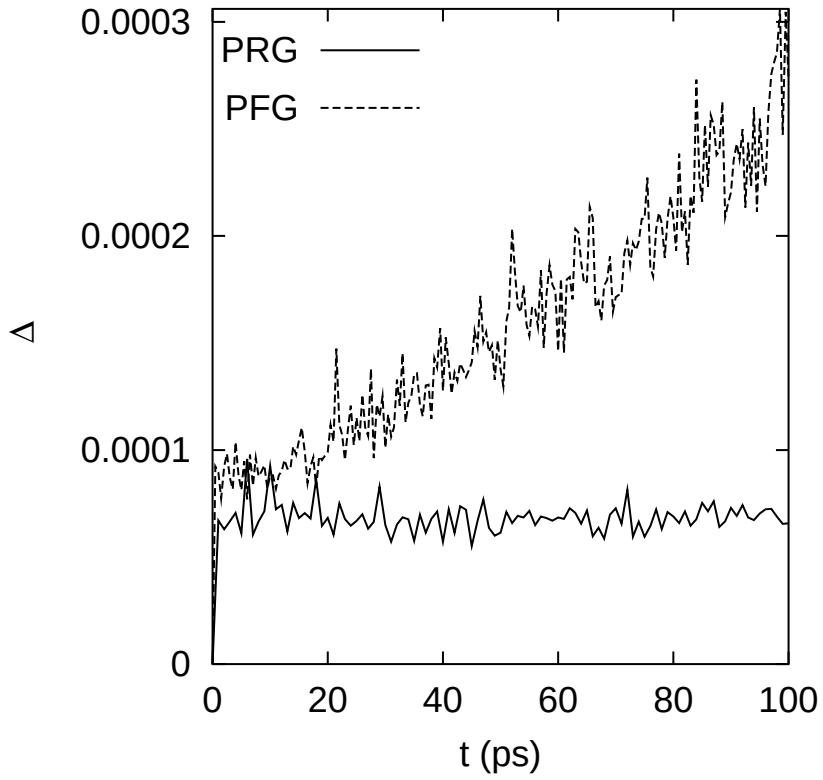

FIG. 6: Estimated errors in the extended-Lagrangian wavefunction as a function of time. The quantity Δ is defined in Eq. (6.1) and measures the magnitude of the error.